Concept for a membrane DBR laser using active/passive regrowth

Vadim Pogoretskiy, Aura Higuera-Rodriguez, P.J. van Veldhoven, Jos J.G.M van der Tol, Dominik Heiss, Meint K. Smit

COBRA Research Institute, Technische Universiteit Eindhoven,
De Zaale, 5600 MB Eindhoven, The Netherlands

For an InP membrane integration platform, a DBR laser is proposed. It is based on butt-joint coupling of the active area to a waveguide. This approach uses selective area regrowth. Design and simulation of the laser as well as successful regrowth results are presented in this paper.

Introduction

In today's big data centers we observe a steady increase of power consumption and data transmission capacity. To keep up with this trend a lot of effort has been made towards integration of photonic components that enables transceivers with small footprint and high power efficiency. Significant advances have been made in silicon photonics using twin-guide structures [1], [2], [3] as well as in InP based technology [4] and III-V membrane technology using a multi regrowth approach [5]. Based on the InP Membrane On Silicon (IMOS) [6] platform we want to propose a technology for small footprint and high density integration using a single selected area regrowth step, where active devices and passive waveguides are directly butt-coupled. In this manuscript we discuss the design and simulation of an integrated DBR laser using this technology. Additionally, we present first successful results of the selective area regrowth.

Laser Design

In the following we discuss the design of the semiconductor optical amplifier (SOA) and distributed Bragg reflectors (DBR) using top-etched gratings.

The geometry of SOA layer stack is shown as schematic cross-section in Fig. 1. It consist of a p-i-n double heterostructure diode which is bonded to a silicon carrier using BCB. The heterostructured design with a InP cladding and a InGaAs active region provides electrical and optical confinement.

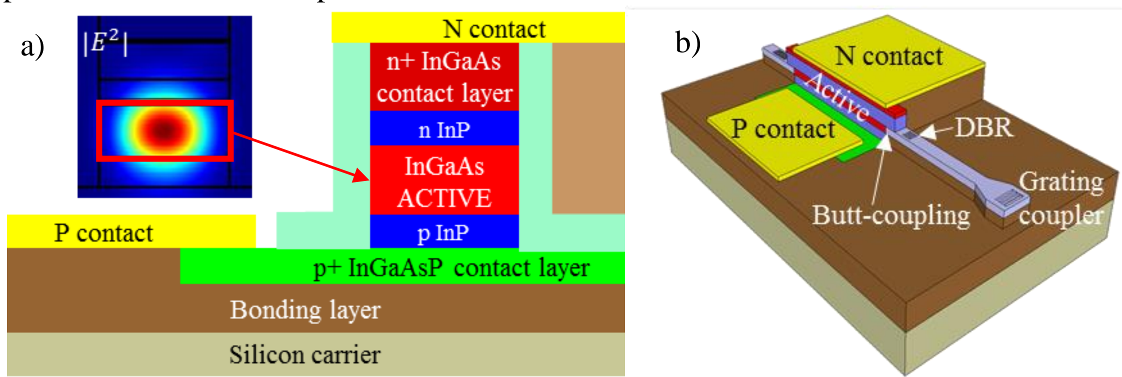

Fig. 1. (a) Cross-section of a SOA; (b) schematic of the butt-coupled DBR Laser.

We use bulk active material which allows us to reach higher modal gain numbers compared to quantum wells and could make ultra-short laser designs possible in the future [7]. To achieve good n- and p- Ohmic contacts we introduce highly doped ternary and quaternary layers, respectively. Metallisation is planned with a low optical loss contact containing Germanium and Silver [8] in the case of the n-contact and Ti-Pt-Au for the p-contact.
In order to optimize the width of the SOA we calculate optical loss and mode confinement in the layerstack as a function of the laser width, which is presented in Fig. 2a. With increasing width the losses decrease saturating at 30 cm^{-1}, while the confinement increases to 0.7 at a width of 2 µm. However, only for widths below 1 µm we observe clear single mode behaviour. We estimate the gain in the SOA by calculating the charge carrier density as a function of current density in our layer stack with self-consisted Poisson calculations and deducing the gain with Fermis golden rule according to reference [9] using a momentum matrix element of $2|M|^2/m_0$=25.3 eV and a temperature of 300 K. Carrier recombination via surface recombination ($v_s=10^5$ cm/s [9]), radiative recombination ($10^{10} cm^3/s$ [9]) and Auger recombination ($7{\cdot}10^{-29}$ cm^6/s [9]) is considered in the model. The resulting modal gain is plotted in Fig. 2b as a function of current density for a laser width of 1 µm. The dashed line shows the maximum available gain, while the continuous line shows the gain at 1550 nm. At 1550 nm a gain of 100 cm^{-1} can be reached with an injection of 11 kA/cm².

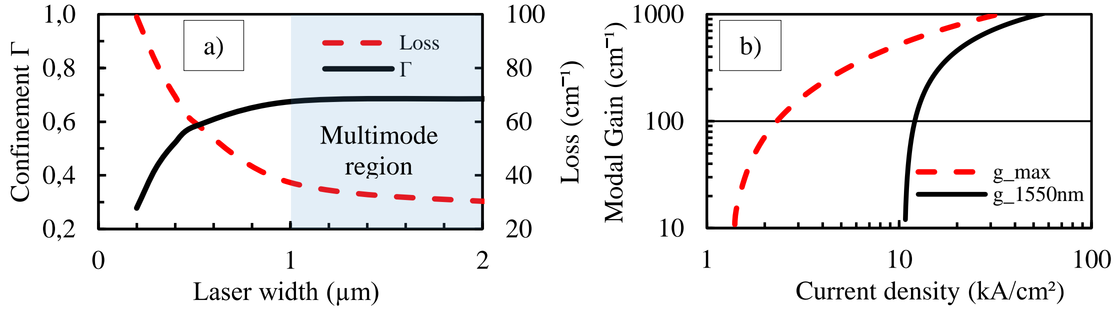

Fig. 2. (a) Optical loss and mode confinement depending on laser width; (b) Modal gain depending on injecting current density with 1 µm laser width.

The SOA can be butt-coupled with a power coupling coefficient exceeding 0.96 to passive high contrast waveguides consisting of a 300 nm thick InP membrane surrounded by polymer (n=1.54). In the passive waveguides we can realize highly efficient on-chip DBRs by etching gratings in the top surface. We simulated the reflectivity of gratings with 300 nm periodicity for etch depths ranging from 100-140 nm using FDTD simulations. The results are presented in Fig. 3.

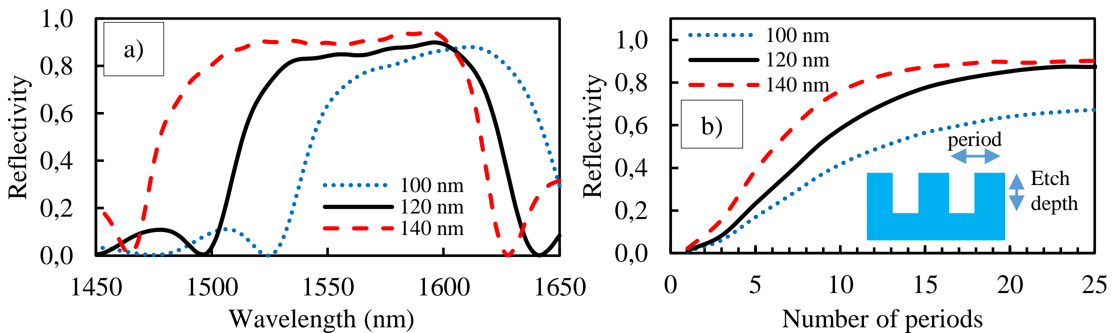

Fig. 3. Reflectivity wavelength (a) and number of periods at 1550nm (b) dependence of DBR mirrors for different etching depth.

Fig. 3a shows the spectral response for 20 periods and Fig. 3b shows the length dependence at 1550 nm. A wide reflection band around 1550 nm can be achieved for a etch depth between 120-140 nm. The strength of the reflection can be continuously tuned up to 90% by choosing the number of periods.

Finally, we will use the presented characteristics to estimate the laser performance regarding threshold current, direct modulation frequency and wall-plug efficiency.

In Fig. 4a we present the threshold current as a function of laser length for different mirror reflectivities and SOA width of 1 µm. The increase of threshold current for short lengths below 30 µm arises from an increased threshold gain due to mirror losses. For lengths exceeding 100 µm the threshold current increases linearly due to the growth of the active region volume. For all of the reflectivity numbers we can achieve low threshold current below 10 mA with SOA length up to 50 µm. Fig. 4b shows direct modulation frequency as a function of length for different output power with 1 µm SOA width and 80% mirror reflectivity. 10 GHz frequency is achievable for high output power and cavity lengths below 100 µm. Fig. 4c depicts wall-plug efficiency as a function of laser length for different output power and reflectivities. For an output power of 1 mW and SOA lengths below 50 µm we achieve a high wall-plug efficiency of 10-15%.

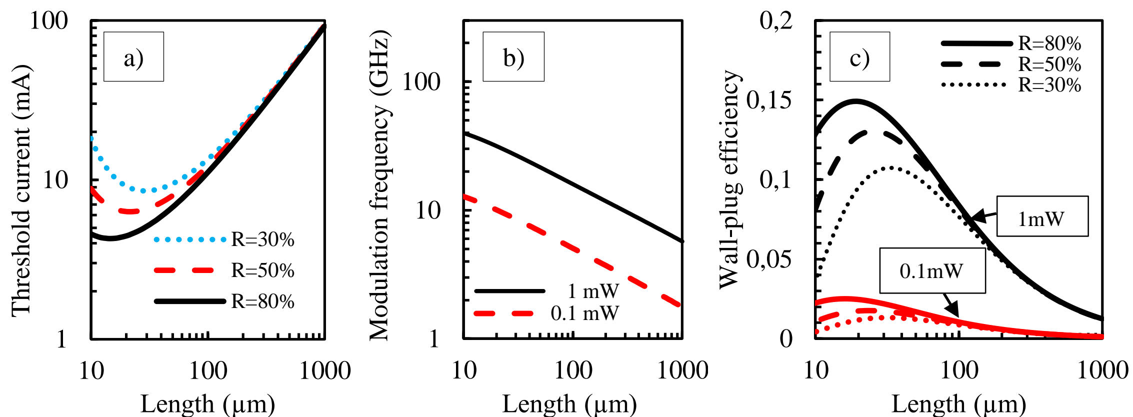

Fig. 4. (a) Threshold current and dependence on laser length with laser width of 1 µm, and with different reflectivity of DBR mirrors; (b) 3dB modulation bandwidth dependence on laser length for different output power and reflectivity of 80%; (c) wall-plug efficiency dependence on laser length for different power and reflectivities.

All above mentioned numbers are valid if we use direct coupling to a waveguide realized with selective area regrowth which we will describe in the section below.

Selective area regrowth

Essential for this design is the selective area regrowth followed by the wafer bonding process. Here, we first grow the active layer stack on top of a (100)-InP wafer. Then, we pattern active areas with 30 µm width and various length by optical lithography and do a combination of dry and wet etching. Finally, we regrow a 300 nm thick InP infill layer for the passive regions of the chip. On the active regions a 400 nm thick Si_xN_y mask prevents further growth. We characterize the regrowth by crossectional SEM images shown on Fig. 5.

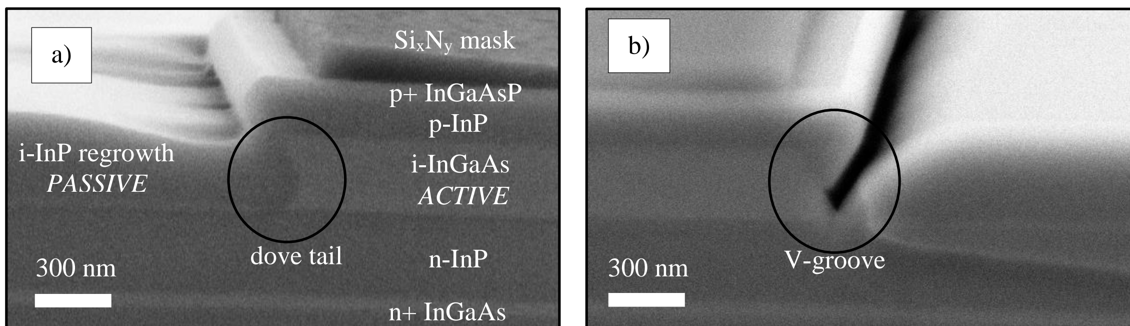

Fig. 5. SEM image of $(0\bar{1}\bar{1})$ facet (dove tail) (a) and $(01\bar{1})$ facet (V-groove) (b).

As a result of wet etching process the $(0\bar{1}\bar{1})$ and $(01\bar{1})$ facets are shaped differently, typically characterized as dove tail and V-grove facet [10]. In the crossectional SEM we observed gap (Fig. 5b) for the V-grove facet. This facet of the ternary compound does not allow InP to nucleate on its surface creating the gap, which prevents light coupling. The dove tail facet, on the other hand, provides a homogeneous interface suitable for active-passive coupling, as shown in Fig. 5a.

Conclusion

In this work we have presented the concept of butt-coupled DBR laser for an InP membrane integration platform (IMOS) which promises good performance parameters for interconnect applications. Concept allows laser designs below 50 µm length with threshold currents below 10 mA, wall-plug efficiency exceeding 10% and a small signal response above 10 GHz. The technology relies on an active-passive regrowth step to make compact, fast and efficient device designs possible. First fabrication trials of active/passive regrowth were successfully performed.

Acknowledgements

We would like to thank the all members of Photonic Integration group for useful discussions, nanolab at TU/e for provided fabrication facilities and research grant Zwaartekracht.

References

[1] H. Park and J. E. Bowers, “Device and integration technology for silicon photonic transmitters,” *IEEE J. Sel. Top. Quantum Electron.*, vol. 17, no. 3, pp. 671–688, 2011.
[2] M. Lamponi and G. H. Duan, “Low-threshold heterogeneously integrated InP/SOI lasers with a double adiabatic taper coupler,” *IEEE Photonics Technol. Lett.*, vol. 24, no. 1, pp. 76–78, 2012.
[3] Y. Jhang, K. Tanabe, S. Iwamoto, and Y. Arakawa, “InAs/GaAs Quantum Dot Lasers on Silicon-on-Insulator Substrates by Metal-Stripe Wafer Bonding,” *IEEE Photonics Technol. Lett.*, vol. 27, no. 8, pp. 875–878, 2015.
[4] M. Smit, and all, “An introduction to InP-based generic integration technology,” *Semicond. Sci. Technol.*, vol. 29, no. 8, p. 083001, 2014.
[5] D. Inoue and S. Arai, “Sub-milliampere threshold operation of butt-jointed built-in membrane DFB laser bonded on Si substrate,” *Opt. Express*, vol. 23, no. 6, p. 7771, 2015.
[6] G. Roelkens, and all, “Photonic integration in indium-phosphide membranes on silicon,” *IET Optoelectron.*, vol. 5, no. 5, pp. 218–225, 2011.
[7] D. Heiss, A. Higuera-Rodriguez, V. Pogoretskiy, A. Fiore, and M. K. Smit, “Design of an efficient photonic crystal beam laser,” *19h Annu. Symp. IEEE Photonics Benelux Chapter*, vol. 19, no. 4, p. 89880, 2014.
[8] L. Shen and all, “Low-optical-loss, low-resistance Ag/Ge based ohmic contacts to n-type InP for membrane based waveguide devices,” *Opt. Mater. Express*, vol. 5, no. 2, p. 393, 2015.
[9] L. A. Coldren and S. W. Corzine, *Diode lasers and photonic circuits*. 2012.
[10] S. Adachi, “Chemical Etching Characteristics of (001)InP,” *J. Electrochem. Soc.*, vol. 128, no. 6, p. 1342, 1981.